Effect of annealing treatment at 550 °C on ferrite of thermally aged cast austenitic stainless steels and ageing kinetics of reverted cast austenitic stainless steels

R. Badyka, Sébastien Saillet, C. Domain, Cristelle Pareige

Journal of Nuclear Materials 542 (2020) 152530

Contents lists available at ScienceDirect

Journal of Nuclear Materials

journal homepage: www.elsevier.com/locate/jnucmat

Effect of annealing treatment at 550 °C on ferrite of thermally aged cast austenitic stainless steels and ageing kinetics of reverted cast austenitic stainless steels

R. Badyka [a,b,*], S. Saillet [b], C. Domain [b], C. Pareige [a]

[a] Groupe de Physique des Matériaux, UMR 6634 CNRS, Université de Rouen Normandie et INSA de Rouen Normandie, France, Avenue de l'université, 76801 St Etienne du Rouvray – France

[b] EDF Lab Les Renardières, MMC Department, F-77818 Moret sur Loing, France

ARTICLE INFO

Article history:
Received 24 March 2020
Revised 19 August 2020
Accepted 10 September 2020
Available online 15 September 2020

Keywords:
Cast austenitic stainless steels
Atom probe tomography
Spinodal decomposition
G-phase precipitation
Annealing treatment

ABSTRACT

Ageing of Cast Austenitic Stainless Steels (CASS) was attributed to the decomposition of the ferrite by spinodal decomposition and precipitation of G-phase particles. This leads to an increase in hardness and a decrease in Charpy-impact energy. It is possible to restore the mechanical properties of these steels by annealing treatment above the Fe-Cr miscibility gap in order to dissolve α' phase. In this work, an annealing treatment for 2 h at 550 °C followed by water quenching was applied to various Mo-free and Mo-bearing steels. This treatment allowed to restore almost completely the mechanical properties of Mo-free steels and partly Mo-bearing steels regardless of the initial ageing time. The mechanical property changes were attributed to the complete dissolution of spinodal decomposition and complete or partial dissolution of G-phase particles. After annealing, a re-ageing kinetics was studied. The preexisting G-phase particles have minor influence on the kinetic of spinodal decomposition until 2,400 h at 400 °C.

1. Introduction

Some components of Light Water Reactors (LWR) were made in cast austenitic stainless steels (CASS). The mechanical properties of these steels evolve at service temperature (285 °C-323 °C) because of the ferrite decomposition into three phases: α (Fe rich) and α'(Cr rich) phases via spinodal decomposition and G-phase via precipitation [1–4]. The ageing leads to a decrease in toughness and an increase in hardness. Our previous work [3], showed that spinodal decomposition and G-phase precipitation at the α/α 'interfaces have similar contribution to hardening in Mo-free steels aged in the (323 °C –350 °C) range in the first part of the kinetics (up to 30,000 h at 350 °C or 200,000 h at 323 °C). In Mo-bearing steels, G-phase precipitation at the α/α' interfaces is the main contributor to ferrite hardness increase because of its high number density ($>10^{24}\ m^{-3}$). Consequently, to restore the mechanical properties, one possibility is to anneal CASS at temperatures high enough to dissolve these phases.

For 25–30 wt% Cr contents, the upper limit of the α-α' miscibility gap of the binary Fe-Cr system is around 520 °C [5]. It is therefore possible to dissolve α and α' phases formed by spinodal decomposition by annealing the material at a temperature greater than 520 °C as shown by Chung et al. [4,6], Li et al. [7] and Danoix et al. [8] who performed annealing at 550 °C and 600 °C [4,6–8]. Nevertheless, at these temperatures, large G-phase particles were still observed. After annealing of Mo-free steels, the dissolution of α and α' zones permitted to restore completely the mechanical properties (Charpy-impact energy, hardness) of the material whatever the initial ageing time and ageing temperature [4,6,7]. The authors concluded that the low density of large G-phase particles observed by Transmission Electron Microscopy (TEM) did not affect hardening. For Mo-bearing steels, two behaviors depending on the initial ageing temperature were observed after annealing. Mechanical properties (Charpy-impact energy, hardness) of alloys aged at 400 °C, were partially recovered due to a total dissolution of spinodal decomposition and a partial dissolution of G-phase particles [8,9]. Mechanical properties of alloys aged at 350 °C were completely restored due to the total dissolution of α/α' decomposition and G-phase particles.

Increase of the annealing temperature could be a solution to dissolve all G-phase particles, but other phases such as the σ or χ phases can precipitate, resulting in an undesirable loss of ductility. Knowing the influence of the small G-phase particles appearing at the α/α' interfaces on the mechanical properties depending on their number density [3] it is therefore necessary to

* Corresponding author.
E-mail address: cristelle.pareige@univ-rouen.fr (R. Badyka).

https://doi.org/10.1016/j.jnucmat.2020.152530
0022-3115/

Table 1
Chemical composition in wt%. The volume fraction of ferrite (δ(%)), thermal ageing treatments (ageing, annealed and re-ageing) are also given.

CASS (wt%)	Cr	Si	Ni	Mo	Mn	C	Fe	δ(%)	Ageing time intervals (h)	Ageing temperature (°C)
B-350 [11] *(Mo-bearing)*	20.08	1.12	11.68	2.49	0.81	0.03	Bal.	17	200,000	350
B-350 [3] *(Mo-bearing)*									200,000 h at 350 °C + 2 h at 550 °C	
C-400 *(Mo-free)*	20.30	0.95	8.40	0.04	0.84	0.03	Bal.	12	2400	400
C-400 *(Mo-free)*									2400 h at 400 °C + 2 h at 550 °C	
E-350 [3] *(Mo-free)*	19.87	0.81	8.47	0.18	0.44	0.03	Bal.	13.5	200,000	350
E-350 *(Mo-free)*									200,000 h at 350 °C + 2 h at 550 °C	
G-400 [3] *(Mo-bearing)*	21.68	0.94	9.61	2.64	0.82	0.03	Bal.	28.5	2400	400
G-400 [3] *(Mo-bearing)*									2400 h at 400 °C + 2 h at 550 °C	
G-400 *(Mo-bearing)*									2400 h at 400 °C + 10 h at 550 °C	
									2400 h at 400 °C + 2 h at 550 °C + 300 h and 2400 h at 400 °C	

investigate the effect of annealing on the G-phase particles at the nanometric scale. Moreover, it is important to quantify the effect of pre-existing G-phase particles (not fully dissolved by the annealing treatment) on the re-ageing kinetics. Indeed, if the G phase particles still present after dissolution cause an acceleration of the kinetics, the interest of the annealing could be limited.

The aims of this paper are to study on one hand the effect of an annealing treatment at 550 °C on the microstructure and microhardness of the ferrite of Mo-bearing and Mo-free steels, and on the other hand the kinetics of phase separation during re-ageing after the annealing treatment in Mo-bearing alloys.

2. Materials and methods

2.1. Materials

Mo-free and Mo-bearing steels were provided by Electricité de France (EDF). A first homogenizing heat treatment were applied around 1100 °C during several hours to fix the ferrite content. Once the duplex structure obtained, the alloys were aged at different temperatures for different ageing times. Compositions and thermal ageing treatments were provided in Table 1 together with the volume fraction of ferrite. The volume fraction of ferrite was calculated in function of alloy composition using the formula proposed by Bonnet et al. [10]. In the following, the term annealing treatment was choosing to refer to the heat treatment performed to restore mechanical properties of aged steels. *Re*-ageing refers to ageing of materials which were annealed (heat treatment after full/partial recovery of mechanical properties). An annealing treatment, consisting of a 2 h holding at 550 °C followed by water quenching, was performed on alloys that previously underwent ageing treatments of 200,000 h at 350 °C or 2400 h at 400 °C. *Re*-ageing of annealed alloys was subsequently performed at 400 °C. The microstructural characterization of B-350 aged at 200,000 h at 350 °C was performed by Pareige et al. [11] and E-350 aged at 200 000 h at 350 °C, G-400 aged at 2400 h at 400 °C and B-350 annealed 2 h at 550 °C by Badyka et al. [3].

2.2. Methods

2.2.1. Microstructural characterization

Atom probe tomography (APT) analyses of the ferrite of the alloy were conducted using a high resolution local electrode atom probe, LEAP 4000 HR (CAMECA). During experiments, specimens were cooled down to 45–50 K in order to avoid preferential field evaporation of chromium. Atoms were evaporated by applying an electric pulse of 20% of the DC voltage with a pulse repetition rate of 200 kHz and with a detection rate equal to 0.3%. The detector efficiency is 36%. The basic principle of APT technique may be found in different books or articles [12–14]. APT samples were prepared either by focus ion beam (FIB) or by standard electropolishing methods. 3D reconstructions were performed using IVAS software (CAMECA) and the data were analysed using the three-dimensional data software for atom probe users developed by GPM Rouen, France. For reconstruction, an image compression factor equal to 1.5 and a field factor value ranging between 3.6 and 5 (depending of the analysed sample and on the fact that samples were on micro-coupon or not) were used. Field factor values were adjusted so as interplanar distances corresponding to the detected crystallographic directions are correct for each experiment.

Characterization of the microstructure was performed with the same parameters as in [3]. Spinodal decomposition is characterized by its wavelength and amplitude. The mean wavelength of the spinodal decomposition (λ) was estimated using autocorrelation functions calculated from 1D Cr concentration profiles [15]. The profiles were drawn by extracting volumes of square cross section of $1 \times 1 nm^2$ from the whole analysed volume and by moving a $1 \times 1 \times 1$ nm^3 box along the z axis with a step value of 0.1 nm. The mean wavelengths have been calculated over at least 50 concentration profiles for each APT volume and from at least three different tips for each condition. The wavelengths were derived from the first two peaks of each auto-correlation profile. The uncertainty on the wavelengths is equal to twice the standard deviation calculated over more than 300 values of wavelength per condition. The amplitude of spinodal decomposition is defined by $\Delta Cr = C_{Cr\alpha'} - C_{Cr\alpha}$, where $C_{Cr\alpha'}$ and $C_{Cr\alpha}$ are the Cr concentration in α' and α zones respectively. Composition of α' and α zones was derived using the method proposed by Zhou et al. [16]. Regarding G-phase precipitation, the radius of the particles and the number density were calculated for each analysis. A concentration filter named isoconcentration [13,17,18] was applied to isolate G-phase particles from α and α' regions using the concentration threshold $X_{Ni+Si+Mn+Mo} > 15\%$. This threshold corresponds to the value for which the concentration histogram of the randomized data set of same composition is negligible ($< 0.01\%$) [17]. As a consequence of the filtering procedure, Fe shells are sometimes observed around

Table 2
Hardness of the ferrite of different CASS before (t = 0 h) and after thermal ageing (t_V).

Steel	Family	State	$HV_{0.05}$ (t = 0 h)	$HV_{0.05}$ (t_v)
B-350 [11]	*Mo-bearing*	200,000 h at	293 ± 34	774 ± 32
E-350 [3]	*Mo-free*	350 °C	230 ± 18	484 ± 53
G-400 [3]	*Mo-bearing*	2400 h at 400 °C	300 ± 18	597 ± 52
C-400 [3]	*Mo-free*		256 ± 18	347 ± 34

particles. These shells were removed using an erosion method. Once the Fe shells were removed, the Guinier radius (R_G) of each individual particle was calculated. The average value is calculated over all the particles detected i.e. more than 200 particles per condition. For more information on the atom-probe characterization procedure, refer to Lefebvre et al. [13]. The number density of the G-phase particles was determined by the ratio of the number of the observed precipitates to the overall analysed volume. The in-core composition of the G-phase particles was obtained from the plateau observed on the erosion profiles. (i.e. the concentration of the particles does not depend on the threshold, the interface is not considered in the measurement).

2.2.2. Microhardness characterization

Microhardness measurements were performed with the following the procedure. For each sample, thirty measurements were performed in ferrite grains with Vickers indenter with a load of 50 g and a dwell time equals to 15 s. Mean and standard deviation were calculated over the 10 highest values. A threshold was defined by substracting three times the standard deviation from the mean hardness value. Only the measurements above this threshold were considered for the final calculation. A minimum of 15 values is mandatory. The final average microhardness value (HV0.05) and the final standard deviation value were calculated over the selected measurements (the uncertainty is equal to twice standard deviation). This method allows excluding the lower hardness values influenced by austenite.

3. Annealing treatment: results and discussion

3.1. Microhardness measurements

Table 2 reports microhardness values of the ferrite in the as-received state (t = 0 h) and for Mo-bearing and Mo-free steels aged 200,000 h at 350 °C and 2400 h at 400 °C. Microhardness values of ferrite of the same alloys after annealing treatment 2 h and 10 h at 550 °C are presented in Table 3. After annealing treatment, the ferrite microhardness of Mo-free steels is close to the unaged ferrite microhardness. This is not the case for the ferrite microhardness of Mo-bearing steels which remains slightly higher for alloys aged at 350 °C and significantly higher for alloys aged at 400 °C. Annealing treatment of 10 h at 550 °C does not improve much restoration when compared to 2 h.

3.2. Atom probe characterization

Fig. 1 presents 3D reconstructions obtained by APT of the ferrite of E-350 and G-400 alloys after thermal ageing and annealing treatment. Table 4 reports the wavelength and amplitude of the spinodal decomposition together with particle radius and number density of G-phase particles before and after annealing treatment for all the investigated alloys. Table 5 provides composition of G-phase particles after thermal ageing and annealing treatment. As already published in [18,19], spinodal decomposition (as shown by Cr distribution) and G-phase precipitation (as shown by Ni+Si+Mn distribution) are observed at α/α' interface.after thermal ageing in the ferrite of alloys E-350 and G-400 (Fig. 1). Before annealing, ferrite of alloy B-350 is the most decomposed (Table 4). G-phase number density is four times higher in Mo-bearing B-350 than in Mo-free E-350 for the same ageing time (after 200,000 h at 350 °C [3,11]). The number density of G-phase particles is similar in both Mo-free E-350 aged 200,000 h at 350 °C and Mo-bearing G-400 aged 2400 h at 400 °C but their size is twice as large after ageing at 400 °C. Concentration of Ni, Si and Mn i.e., G-former elements, (Table 5) is higher in G-phase particles of Mo-bearing alloys, the highest level being observed for the Mo-bearing alloy aged at 400 °C. So, at 400 °C, G-former elements concentrations and particles radius are the largest. Spinodal decomposition is quite similar for all the alloys.

After annealing treatment, the 3D elemental maps of Cr (Fig. 1) in the ferrite of E-350 and G-400 alloys are uniform, showing the complete dissolution of the spinodal decomposition at this temperature. Similar results were obtained for all the investigated alloys (Table 4). Regarding G-phase precipitation, G-phase particles totally dissolved in the case of Mo-free alloys (Table 4 and Fig. 1). Conversely, G-phase particles still remain in the ferrite of Mo-bearing alloys after annealing for 2 h at 550 °C (Table 4 and Fig. 1) although with a lower number density. The decrease in number density could be associated either to the coarsening of the particles or to their dissolution. The fact that the radius does not increase is in favour of the dissolution of the particles. Results show that the annealing treatment of 10 h at 550 °C is unable to dissolve the remaining G-phase particles.

The core composition of the G-phase particles was also modified by the annealing treatment but trends are difficult to draw. Whereas a decrease of 8 at% in Ni was observed for the Mo-bearing G-400 after annealing, no variation in Ni content was observed for the Mo-bearing B-350 (Table 5). Mo was observed to enrich G-phase particles after annealing. After 10 h of annealing, the G-phase particles were found to increase their Ni (+ 4 at%), Si (+ 3 at%) and Mo (+1 at%) content compared with values observed after 2 h of annealing. This decrease in Ni concentration and afterwards increase after 8 h of additional annealing is surprising. We do not have any explanation at this point.

3.3. Discussion

Annealing treatment enables the recovery of at least 70% of microhardness of the ferrite of the CASS whatever the initial thermal

Table 3
Hardness of the ferrite of different cast austenitic stainless steels after annealing treatment of 2 h at 550 °C and 10 h at 550 °C.

Steel	Family	State	$HV_{0.05}$ (t = 0 h)	$HV_{0.05}$ (annealing)
B-350	*Mo-bearing*	*200,000 h at 350 °C* + 2 h at 550 °C	293 ± 34	315 ± 43
E-350	*Mo-free*		230 ± 18	227 ± 53
C-400	*Mo-free*	*2400 h at 400 °C* + 2 h at 550 °C	256 ± 18	224 ± 14
G-400 [3]	*Mo-bearing*		300 ± 18	384 ± 59
G-400	*Mo-bearing*	*2400 h at 400 °C* + 10 h at 550 °C	300 ± 18	352 ± 28

Table 4
Characteristic parameters of spinodal decomposition and G-phase particles obtained by atom probe tomography for the alloys of Table 1 together with their microhardness increase. Averaged over at least 200 G-phase particles per condition.

Alloy	Family	Ageing (h and °C)	Spinodal decomp.		G-phase particles		$\Delta HV\alpha_{0.05}$
			ΔCr (at%)	λ (nm)	Number density ($x10^{23} m^{-3}$)	R_G (nm)	
B-350 [11]	*Mo-bearing*	200,000 h at 350 °C	58.4 ± 1.1	6.5 ± 0.6	41.0 ± 5.0	1.6 ± 0.2	481±66
E-350 [3]	*Mo-free*	200,000 h at 350 °C	51.1 ± 0.3	5.1 ± 1.1	9.7 ± 1.0	1.5 ± 0.8	254±71
G-400 [3]	*Mo-bearing*	2400 h at 400 °C	51.1 ± 0.3	5.4 ± 0.9	9.9 ± 0.2	3.0 ± 0.9	297±70
C-400	*Mo-free*	2400 h at 400 °C	No atom probe data				91±43
B-350	*Mo-bearing*	200,000 h at 350 °C + Annealed 2 h at 550 °C	Dissolved		2.5 ± 0.3	1.9 ± 0.7	23±77
E-350	*Mo-free*	200,000 h at 350 °C + Annealed 2 h at 550 °C			Dissolved	Dissolved	0 ± 53
G-400 [3]	*Mo-bearing*	2400 h at 400 °C + Annealed 2 h at 550 °C			4.4 ± 0.2	2.3 ± 0.6	84±77
C-400	*Mo-free*	2400 h at 400 °C + Annealed 2 h at 550 °C			Dissolved	Dissolved	0 ± 77
G-400	*Mo-bearing*	2400 h at 400 °C + Annealed 10 h at 550 °C			2.5 ± 0.2	2.1 ± 1.4	52±46

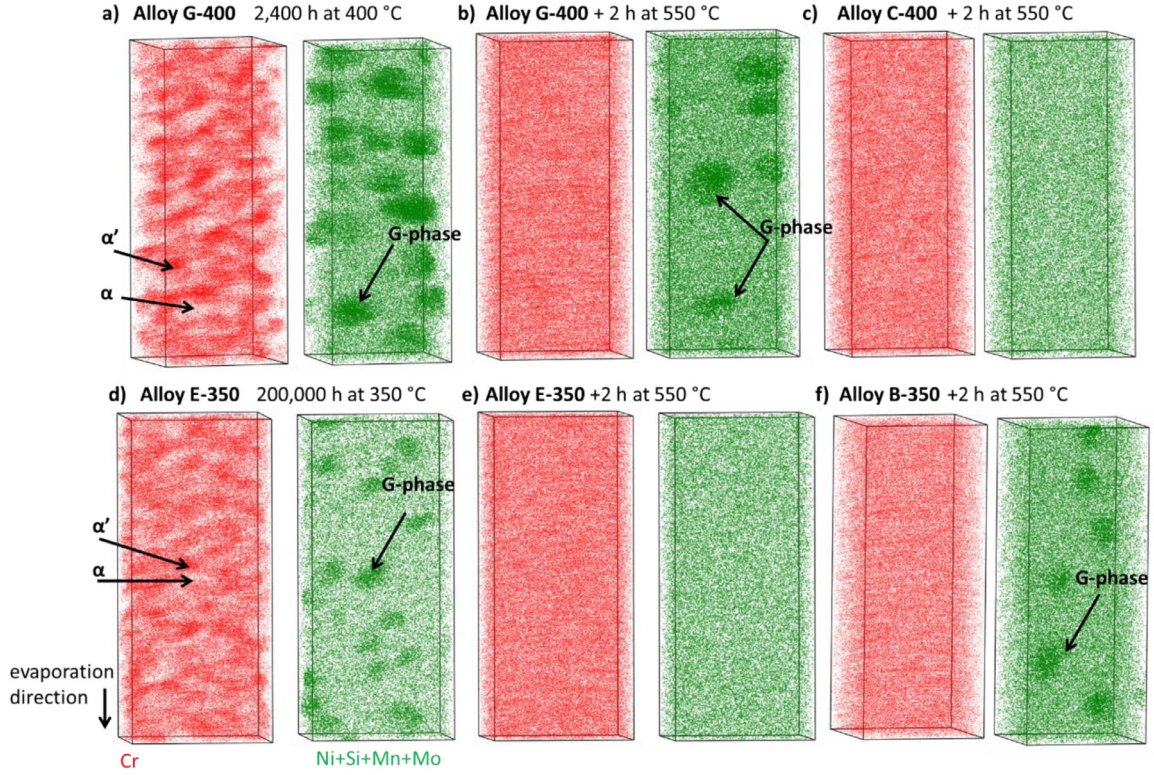

Fig. 1. Cr atom distributions (red) and Ni+Si+Mn+Mo atom distributions (green) obtained by atom probe for the ferrite of alloy G-400 (a) after 2400 h at 400 °C, (b) after 2400 h at 400 °C + annealing treatment and for the ferrite of alloy C-400 (c) after 2400 h at 400 °C + annealing treatment. Same atom distribution for the ferrite of alloy E-350 (d) after 200,000 h at 350 °C and (e) after 200,000 h at 350 °C +annealing treatment and for the ferrite of alloy B-350 (f) after 200,000 h at 350 °C + annealing treatment. $V = 20 \times 20 \times 50$ nm^3. (For interpretation of the references to colour in this figure legend, the reader is referred to the web version of this article.)

ageing ($\leq$ 200,000 h at 350 °C and $\leq$ 2400 h at 400 °C). In good agreement with the literature [4,6–8]:

- There is a total dissolution of the spinodal decomposition after annealing treatment of 2 h at 550 °C;
- The annealing treatment allows to fully restore microhardness of Mo-free steels whatever the initial ageing temperature and even for very long ageing time (200,000 h). Contrary to the literature [4,6,7], in this study, all G-phase particles were dissolved by the annealing treatment whatever the ageing temperature. Both spinodal decomposition and G-phase particles being dissolved, a full recovery of the microhardness is observed;
- The annealing treatment only permits to partly recover the microhardness of Mo-bearing steels. Presence of G-phase particles with a number density of 2–4 $\times$ 10^{23} m^{-3} explains the absence of a total recovery of the mechanical properties [3]. These results confirms the significant contribution of these particles to hardening as reported by different authors [3,4,8].

Comparison of the behaviour of Mo-free with Mo-bearing steels suggest that dissolution of G-phase particles is more difficult in Mo-bearing steels. This could be due to differences in crystallographic structure and/or composition.

At 350 °C after 200,000 h of ageing, the G-phase particles in Mo-bearing steels present higher concentration in G-former elements Ni (+2 at%), Si (+4 at%), Mn (+3 at%) and of course into Mo (+5 at.%) than in Mo-free steels. At 400 °C, the highest stability of G-phase particles could also be due to the increase in G-former content. As illustrated in Fig. 2, the thermal stability limit of G-phase in Mo-free steels due to Mo and Ni content is lower than the thermal stability limit of G-phase in Mo-bearing steels. These thermodynamic calculations were performed with MatCalc

Table 5
G-phase particles composition (at%) obtained by atom probe after thermal ageing and annealing treatment (Averaged over at least 200 G-phase particles per condition.).

Steels	Ageing (h and °C)	Ni	Si	Mn	Mo	Cr	Fe	P
B-350 [11] (*Mo-bearing*)	200,000 h at 350 °C	33.20 ± 1.50	16.10 ± 1.20	6.80 ± 0.80	5.20 ± 0.70	9.60± 0.90	28.4 ± 1.5	0.7 ± 0.3
E-350 [3] (*Mo-free*)	200,000 h at 350 °C	31.53 ± 0.52	11.75 ± 0.38	3.81 ± 0.23	0.37 ± 0.07	11.16 ± 0.37	40.83 ± 0.68	0.4 ± 0.1
G-400 [3] (*Mo-bearing*)	2400 h at 400 °C	39.75 ± 0.61	18.25 ± 0.48	10.06 ± 0.38	6.43 ± 0.31	8.58 ± 0.35	15.53 ± 0.45	0.9 ± 0.1
B-350 (*Mo-bearing*)	Annealed 2 h at 550 °C	33.2 ± 1.8	19.8 ± 1.6	6.9 ± 0.9	9.2 ± 1.1	13.7 ± 1.3	14.7 ± 1.4	1.40±0.50
E-350 (*Mo-free*)	Annealed 2 h at 550 °C	Dissolved G-phase particles						
G-400 [3] (*Mo-bearing*)	Annealed 2 h at 550 °C	31.7 ± 0.6	18.5 ± 0.5	8.5 ± 0.4	8.1 ± 0.4	13.7 ± 0.4	17.0 ± 0.5	1.48±0.16
C-400 (*Mo-free*)	Annealed 2 h at 550 °C	Dissolved G-phase particles						
G-400 (*Mo-bearing*)	Annealed 2 *h* + 8 h at 550 °C	36.5 ± 1.1	21.4 ± 0.9	7.6 ± 0.6	9.38±0.69	11.6 ± 0.8	11.2 ± 0.7	1.36±0.28

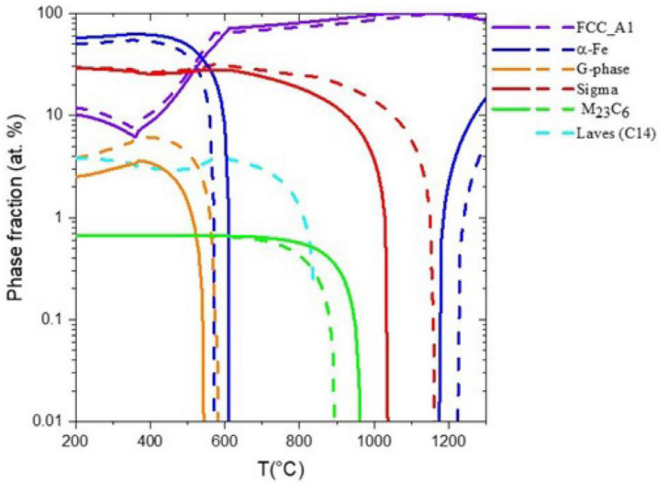

Fig. 2. Predictive equilibrium phase fractions calculation as function of temperature. Dash lines correspond to phase fraction for Mo-bearing steels and continuous lines to phase fraction for Mo-free steels. [20]. (For interpretation of the references to colour in this figure legend, the reader is referred to the web version of this article.)

and a revised and updated database for Fe alloys, with some thermodynamic parameters adjusted on density functional theory calculations for the different possible G phase formation energies, as well as additional intermetallic phases [20].

With upper thermal stability close to 550 °C, the G-phase particle in Mo-bearing steels remain after annealing treatment until 10 h at 550 °C. The thermal stability explanation does not justify the partial dissolution of the G-phase particle in Mo-bearing steels observed.

It could also originate from a change in crystallographic structure or both of them as the change in structure can be associated to the composition evolution [2,21]. Matsukawa et al. [22] and Hamaoka et al. [23,24] showed that G-phase particles structure evolved with ageing time. From the base centred cubic (BCC) at the beginning of the kinetics, G-phase particles become face centred cubic (FCC) at longer ageing time for larger size. This structural change was observed after 2400 h of ageing at 400 °C for Mo-bearing steels [23,24] and after 10,000 h at 400 °C in Mo-free steels [22]. TEM characterization performed by Yamada et al. [9] in Mo-bearing showed that the FCC G-phase particles formed in Mo-bearing steels after 10,000 h at 400 °C are indeed not dissolved by a annealing treatment of 1 h at 550 °C. This could explain the fact that Chung et al. [4,6] and Li et al. [7] observed the G-phase particles in the Mo-free alloys aged 10,000 h at 400 °C. In this paper, G-400 alloy was characterized after 2400 h at 400 °C which is close to the conditions for BCC/FCC transition according to the work of Hamaoka et al. [23,24]. It is thus possible that the remaining G-phase particles after annealing are FCC G-phase particles stable at 550 °C. This would also explain why particles of alloy G-400 annealed during 10 h are not dissolved. Nevertheless, this is in contradiction with the fact that the radius does not increase at this temperature between 2 h and 10 h of annealing treatment. Additional data are needed to conclude on this point. The partial dissolution of G-phase particles in alloy B-350 could also have the same origin. After a thermal ageing of 200,000 h at 350 °C, a part of G-phase particles could have the FCC structure. Unfortunately, only atom probe analyses were carried out and they do not allow the characterization of the crystalline structure. The crystallographic characterization by TEM is one of the perspectives of this work.

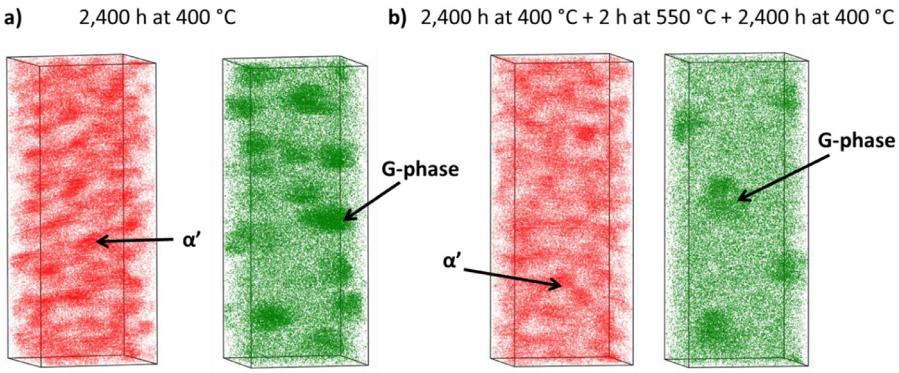

Fig. 3. Cr atoms distributions (red) and Ni+Si+Mn+Mo atoms distributions (green) obtained by APT in ferrite of alloy G-400 (a) after 2400 h at 400 °C and (b) after 2400 h at 400 °C + 2 h at 550 °C + 2400 h at 400 °C. $V = 20 \times 20 \times 50$ nm^3. (For interpretation of the references to colour in this figure legend, the reader is referred to the web version of this article.)

Table 6
Characteristic parameters of spinodal decomposition and G-phase particles obtained by atom probe tomography for the alloys G-400 together with their microhardness increase. $\Delta HV_{0.05} = HV_{t_u} - HV_{t=0}$. Averaged over at least 200 particles per condition.

Alloy	Ageing (h and °C)	Spinodal decomp.		G-phase particles		$\Delta HV\alpha_{0.05}$
		ΔCr (%at)	λ(nm)	Number density (x10^{23}m^{-3})	R_G(nm)	
G-400 [3]	2400 h at 400 °C	51.1 ± 0.3	5.4 ± 0.9	9.9 ± 0.2	3.0 ± 0.9	297±70
G-400 [3]	Annealed 2 h at 550 °C	Dissolved		4.4 ± 0.2	2.3 ± 0.6	84±77
G-400	Annealed 2 *h* + 8 h at 550 °C			2.5 ± 0.2	2.1 ± 1.4	52±46
G-400	Annealed 2 h at 550 °C +Reaged 300 h at 400 °C	31.4 ± 0.3	3.2 ± 0.9	4.2 ± 0.4	2.9 ± 0.6	175±59
G-400	Annealed 2 h at 550 °C +Reaged 2400 h at 400 °C	49.2 ± 0.3	5.0 ± 1.0	3.7 ± 0.2	3.4 ± 0.9	304±99

Table 7
G-phase particle composition (at.%) obtained by APT for alloy G-400 for different ageing conditions (Averaged over at least 200 particles per condition).

Alloys	Ageing (h and °C)	Ni	Si	Mn	Mo	Cr	Fe	P
G-400 (Mo-bearing)	2400 h à 400 °C	39.75 ± 0.6	18.25 ± 0.5	10.06 ± 0.4	6.43 ± 0.3	8.58 ± 0.4	15.53 ± 0.5	0.9 ± 0.1
G-400 (Mo-bearing)	Annealed 2 h at 550 °C	31.7 ± 0.6	18.5 ± 0.5	8.5 ± 0.4	8.1 ± 0.4	13.7 ± 0.4	17.0 ± 0.5	1.48±0.2
G-400 (Mo-bearing)	Annealed + *Re*-aged 300 h at 400 °C	33.7 ± 0.7	16.3 ± 0.6	8.0 ± 0.4	9.8 ± 0.5	13.5 ± 0.6	15.8 ± 0.6	1.6 ± 0.2
G-400 (Mo-bearing)	Annealed +*Re*-aged 2400 h at 400 °C	38.7 ± 0.4	18.8 ± 0.3	8.6 ± 0.2	8.9 ± 0.2	10.5 ± 0.3	12.0 ± 0.3	1.4 ± 0.1

4. Results and discussion of re-ageing treatment

After annealing treatment, re-ageing kinetics were investigated. The goal is to study the effect of pre-existing G-phase particles which are not dissolved during annealing treatment on ageing at 400 °C.

4.1. APT results

Fig. 3 presents the 3D distribution maps of Cr (red) and Ni+Si+Mn+Mo (green) obtained by APT in alloy G-400 after initial thermal ageing and after re-ageing 2400 h at 400 °C. Characteristics of spinodal decomposition and of G-phase particles are reported in Table 6.

The characteristics of the spinodal decomposition are the same after 2400 h at 400 °C and after re-ageing for the same ageing time at the same temperature. Regarding G-particles, some differences are noticed. The radius of G-phase particles is larger after re-ageing and number density smaller which is characteristic of the coarsening regime. Table 7 and Table 8 give the measured composition of particles and of α and α' zones, respectively.

During coarsening, G-phase particles also enrich in Ni and deplete in Cr and Fe. The composition reached after re-ageing is quite close to the composition of particles after the initial thermal ageing. The only differences concern Mn (lower concentration) and Mo (higher concentration). The composition of the α and α' zones shows a decrease in Ni, Si and Mn linked to the precipitation of the phase G particles. For the other elements (Mo, P, Cu, C and V), their concentrations in the α and α' zones remain identical considering the measurement uncertainties.

4.2. Discussion - link with mechanical properties

The spinodal decomposition has the same characteristics with pre-existing G-phase particles than without. This means that the initial G-phase particles have a minor influence on the spinodal decomposition kinetics. G-400 ferrite microhardness and toughness obtained after ageing and re-ageing are provided in Table 9. Due to microstructure (a smaller number density of G-phase particles, for G-400 re-aged), it is expected a greater Charpy-impact energy and a lower micro-hardness for G-400 re-aged than for G-400 aged 2400 h at 400 °C. Nevertheless, given the number of measurements and alloys studied, there is not significant variation in mechanical properties between G-400 2400 h at 550 °C and G-400 annealed and re-aged 2400 h at 550 °C despite a slight variation in the microstructure.

Table 8
α and α' zones composition (at.%) obtained by APT for alloy G-400 for different ageing conditions.

Ageing (h and °C)	Phase	Ni	Si	Mn	Mo	Cr	P	Cu, C and V	Fe
2400 h à 400 °C	α'	2.6 ± 0.1	2.2 ± 0.1	0.4 ± 0.1	2.7 ± 0.1	58.8 ± 0.2	0.06±0.01	0.1 ± 0.1	32.9 ± 0.2
	α	4.3 ± 0.1	0.9 ± 0.1	0.2 ± 0.1	1.3 ± 0.1	7.7 ± 0.2	0.03±0.02	0.2 ± 0.1	85.1 ± 0.2
Annealed + *Re*-aged 300 h	α'	4,7 ± 0.1	2,4 ± 0.1	0,8 ± 0.1	2,5 ± 0.1	43.5 ± 0.2	0.07±0.01	0.2 ± 0.1	45.8 ± 0.2
at 400 °C	α	4,2 ± 0.1	1,4 ± 0.1	0,4 ± 0.1	1,4 ± 0.1	12.1 ± 0.2	0.07±0.01	0.2 ± 0.1	80.2 ± 0.2
Annealed + *Re*-aged	α'	2.8 ± 0.1	2.2 ± 0.1	0.6 ± 0.1	2.6 ± 0.1	56.0 ± 0.2	0.08±0.01	0.1 ± 0.1	35.4 ± 0.2
2400 h at 400 °C	α	3.4 ± 0.1	1.0 ± 0.1	0.2 ± 0.1	1.4 ± 0.1	6.8 ± 0.2	0.07±0.01	0.2 ± 0.1	86.8 ± 0.2

Table 9
Charpy impact-energy and microhardness of the ferrite of different cast austenitic stainless steels after thermal ageing, annealing for 2 h at 550 °C and re-ageing.

Alloys	Ageing treatment	$HV_{0.05}$ ($t = 0$)	$HV_{0.05}$ (t_v)	KCU at 20 °C (da/cm²)
G-400 [3]	2400 h at 400 °C	300 ± 18	597 ± 52	2.5
G-400 [3]	Annealed 2 h at 550 °C		384 ± 59	21.4
G-400	Annealed +*Re*-aged 300 h at 400 °C		475 ± 41	8.0
G-400	Annealed +*Re*-aged 2400 h at 400 °C		604 ± 81	3.7

5. Conclusion

An annealing treatment of 2 h at 550 °C has been applied to some Mo-bearing and Mo-free CASS. The effect of this treatment on the microstructure and microhardness of the ferrite has been investigated. Two behaviors were observed depending on the composition of the steels:

- For Mo-free steels, the microhardness has been fully restored. The recovery is related to the total dissolution of spinodal decomposition and the small G-phase particles formed at the α /α' interfaces;
- For Mo-bearing steels, a partial restoration of the microhardness has been reported. The residual hardness of the ferrite is due to the partial dissolution of G-phase particles, the spinodal decomposition being totally dissolved. It is suggested that this difference in dissolution kinetics of the G phase particles between Mo-bearing and Mo-free steels is related to the difference in composition (and related thermodynamic properties) and or in crystallographic structure of the particles (BCC versus FCC).

In order to investigate the effect of the non-dissolved G-phase particles on kinetics of phase separation, a re-ageing treatment has been applied to restore Mo-bearing alloys. Presence of pre-existing G-phase particles did not influence the spinodal decomposition kinetics. During the re-ageing, preexisting G-particles enter a coarsening regime. Their size is larger and their number density smaller after re-ageing treatment than after the initial thermal ageing.

Declaration of Competing Interest

The authors declare that they have no known competing financial interests or personal relationships that could have appeared to influence the work reported in this paper.

CRediT authorship contribution statement

R. Badyka: Writing - original draft, Investigation, Visualization. **S. Saillet:** Investigation, Writing - review & editing. **C. Domain:** Writing - review & editing. **C. Pareige:** Resources, Writing - review & editing, Supervision.

Acknowledgements

This work contributes to the research program of the EDF-CNRS joint laboratory EM2VM (Study and modeling of the Micro- structure for Ageing of Materials). This work was carried out owing to experimental GENESIS platform. GENESIS is supported by the Région Haute-Normandie, the Métropole Rouen Normandie, the CNRS via LABEX EMC and the French Natonal Research Agency as a part of the program “Investissements d’avenir” with the reference ANR-11-EQPX-0020.

References

[1] P. Auger, F. Danoix, A. Menand, S. Bonnet, J. Bourgoin, M. Guttmann, Atom probe and transmission electron microscopy study of aging of cast duplex stainless steels, Mater. Sci. Technol. 6 (1990) 301–313, doi:10.1179/mst.1990.6.3.301.
[2] A. Mateo, L. Llanes, M. Anglada, A. Redjaimia, G. Metauer, Characterization of the intermetallic G-phase in an AISI 329 duplex stainless steel, J. Mater. Sci. 32 (1997) 4533–4540, doi:10.1023/A:1018669217124.
[3] R. Badyka, G. Monnet, S. Saillet, C. Domain, C. Pareige, Quantification of hardening contribution of G-Phase precipitation and spinodal decomposition in aged duplex stainless steel: APT analysis and micro-hardness measurements, J. Nucl. Mater. 514 (2019) 266–275, doi:10.1016/j.jnucmat.2018.12.002.
[4] H.M. Chung, T.R. Leax, Embrittlement of laboratory and reactor aged CF3,CF8, and CF8M duplex stainless steels, Mater. Sci. Technol. 6 (1990) 249–262, doi:10.1179/mst.1990.6.3.249.
[5] W. Xiong, P. Hedström, M. Selleby, J. Odqvist, M. Thuvander, Q. Chen, An improved thermodynamic modeling of the Fe–Cr system down to zero kelvin coupled with key experiments, Calphad 35 (2011) 355–366, doi:10.1016/j.calphad.2011.05.002.
[6] H.M. Chung, O.K. Chopra, Kinetics and Mechanism of Thermal Aging Embrittlement of Duplex Stainless Steels, Argonne National Lab., ILUSA, 1987 https://www.osti.gov/scitech/biblio/5856937.
[7] S.L. Li, H.L. Zhang, Y.L. Wang, S.X. Li, K. Zheng, F. Xue, X.T. Wang, Annealing induced recovery of long-term thermal aging embrittlement in a duplex stainless steel, Mater. Sci. Eng. A. 564 (2013) 85–91, doi:10.1016/j.msea.2012.11.046.
[8] F. Danoix, P. Bas, J.P. Massoud, M. Guttmann, P. Auger, Atom probe and transmission electron microscopy study of reverted duplex stainless steels, Appl. Surf. Sci. 67 (1993) 348–355, doi:10.1016/0169-4332(93)90337-B.
[9] T. Yamada, S. Okano, H. Kuwano, Mechanical property and microstructural change by thermal aging of SCS14A cast duplex stainless steel, J. Nucl. Mater. 350 (2006) 47–55, doi:10.1016/j.jnucmat.2005.11.008.
[10] S. Bonnet, J. Bourgoin, J. Champredonde, D. Guttmann, M. Guttmann, Relationship between evolution of mechanical properties of various cast duplex stainless steels and metallurgical and aging parameters: outline of current EDF programmes, Mater. Sci. Technol. (1990) 221–229.
[11] C. Pareige, S. Novy, S. Saillet, P. Pareige, Study of phase transformation and mechanical properties evolution of duplex stainless steels after long term thermal ageing (>20 years), J. Nucl. Mater. 411 (2011) 90–96, doi:10.1016/j.jnucmat.2011.01.036.
[12] B. Gault, M.P. Moody, Atom Probe Microscopy, Springer, Springer, n.d.
[13] W. Lefebvre, F. Vurpillot, X. Sauvage, Atom Probe Tomography: Put Theory Into Practice, Academic Press, 2016.
[14] D.J. Larson, TyJ. Prosa, Local Electrode Atom Probe Tomography, Springer, n.d.
[15] M.G. Hetherington, M.K. Miller, Some aspects of the measurement of composition in the atom probe, J. Phys. Colloq. 50 (1989) C8-535-C8-540, doi:10.1051/jphyscol:1989892.
[16] J. Zhou, J. Odqvist, M. Thuvander, P. Hedström, Quantitative evaluation of spinodal decomposition in Fe-Cr by atom probe tomography and radial distribution function analysis, Microsc. Microanal. Off. J. Microsc. Soc. Am. Microbeam Anal. Soc. Microsc. Soc. Can. 19 (2013) 665–675, doi:10.1017/S1431927613000470.
[17] J.M. Hyde, G. DaCosta, C. Hatzoglou, H. Weekes, B. Radiguet, P.D. Styman, F. Vurpillot, C. Pareige, A. Etienne, G. Bonny, N. Castin, L. Malerba, P. Pareige,

Analysis of Radiation Damage in Light Water Reactors: comparison of Cluster Analysis Methods for the Analysis of Atom Probe Data, Microsc. Microanal. 23 (2017) 366–375, doi:10.1017/S1431927616012678.
[18] C. Pareige, J. Emo, S. Saillet, C. Domain, P. Pareige, Kinetics of G-phase precipitation and spinodal decomposition in very long aged ferrite of a Mo-free duplex stainless steel, J. Nucl. Mater. 465 (2015) 383–389, doi:10.1016/j.jnucmat.2015.06.017.
[19] J.D. Tucker, M.K. Miller, G.A. Young, Assessment of thermal embrittlement in duplex stainless steels 2003 and 2205 for nuclear power applications, Acta Mater 87 (2015) 15–24, doi:10.1016/j.actamat.2014.12.012.
[20] A. Jacob, C. Domain, G. Adjanor, P. Todeschini, E. Povoden-Karadeniz, Thermodynamic modeling of G-phase and assessment of phase stabilities in reactor pressure vessel steels and cast duplex stainless steels, J. Nucl. Mater. 533 (2020) 152091, doi:10.1016/j.jnucmat.2020.152091.
[21] F. Danoix, P. Auger, S. Chambreland, D. Blavette, A 3D study of G-phase precipitation in spinodally decomposed α-ferrite by tomographic atom-probe analysis, Microsc. Microanal. Microstruct. 5 (1994) 121–132, doi:10.1051/mmm:0199400502012100.
[22] Y. Matsukawa, T. Takeuchi, Y. Kakubo, T. Suzudo, H. Watanabe, H. Abe, T. Toyama, Y. Nagai, The two-step nucleation of G-phase in ferrite, Acta Mater 116 (2016) 104–113, doi:10.1016/j.actamat.2016.06.013.
[23] T. Hamaoka, A. Nomoto, K. Nishida, K. Dohi, N. Soneda, Effects of aging temperature on G-phase precipitation and ferrite-phase decomposition in duplex stainless steel, Philos. Mag. 92 (2012) 4354–4375, doi:10.1080/14786435.2012.707340.
[24] T. Hamaoka, A. Nomoto, K. Nishida, K. Dohi, N. Soneda, Accurate determination of the number density of G-phase precipitates in thermally aged duplex stainless steel, Philos. Mag. 92 (2012) 2716–2732, doi:10.1080/14786435.2012.674222.